Journal of Fluorescence (2019) 29:1431–1443
https://doi.org/10.1007/s10895-019-02464-3

ORIGINAL ARTICLE

A chemosensoring molecular lab for various analytes and its ability to execute a molecular logical digital comparator

Awad I. Said[1,2] · Nikolai I. Georgiev[1] · Shaimaa A. Hamdan[2] · Vladimir B. Bojinov[1]

Received: 3 September 2019 / Accepted: 6 November 2019 / Published online: 23 November 2019

Abstract

We reported here the unique ability of a Rhodamine 6G-based probe (**3**) to detect discriminately several targets, including H^+, HO^-, Cu^{2+}, Hg^{2+}, Fe^{3+}, Co^{2+}, Cd^{2+}, Zn^{2+}, Sn^{2+}, Ni^{2+}, Al^{3+}, Pb^{2+}, $Ce^{3+}$and Ag^+, by unambiguously colorimetric and fluorimetric outcomes. In aqueous solutions, the presence of proton induced the ring-opening of rhodamine moiety but the presence of hydroxide induced the conversion of 2-hydroxyphenyl hydrazone moiety from the non-fluorescent benzenoid form into the fluorescent quinoid form. The probe could to distinguish between different cations in DMF and to work like an artificial tongue at molecular level. Several logic gates including *OR*, *INHIBIT* and *TRANSFER*, were performed by the probe. Moreover, the probe is able to execute three *INHIBIT* logic gates by two inputs, which was exploited to execute a digital molecular comparator.

Keywords Chemosensoring molecular lab · Multidetection of analytes · Fluorescent probe · Cations · pH · Molecular digital comparator

Abbreviations

HEPES	4-(2-hydroxyethyl)-1-piperazineethanesulfonic acid
DMF	*Dimethylformamide*
NMR	Nuclear magnetic resonance
FT-IR	Fourier transform infrared spectroscopy
UV-VIS	Ultraviolet Visible Spectroscopy

Introduction

pH plays an important role in clinical analysis, food production, wastewaters treatment procedures, environmental and life sciences, etc. [1–5]. Several works confirmed the effect of abnormal pH values on biological processes and its responsibility for many common disease types such as cancer and Alzheimer's [6, 7]. Although a potentiometric pH sensor for routine measurements is well established, it exhibits many drawbacks including miniaturization, disposable devices and work in a strong electromagnetic field [8, 9]. Indeed, fluorescence probes succeed to be an alternative in overcoming the above-mentioned limitations [10–14].

Heavy metal ions are of great concern, not only for the scientific community, but of also concerning many pollution aspects due to health problems associated with it [15–17]. Some metal ions, such as Fe(III), Zn(II), Cu(II), Co(II), and Ni(II) are necessary for the survival of humans. However, high concentrations of these ions can lead to many diseases [18, 19]. Others such as Hg(II), Cd(II), Pb(II) and Sn(II) are among the most toxic elements to human because of their higher affinity to bind to the biomolecules affecting their biological functions [20–22]. Therefore, the development of selective and sensitive methods for detecting heavy metal ions is the focus of the recent research attention [23–25]. There were many traditional methods for detecting the low concentrations of heavy ions, including atomic absorption spectroscopy, plasma atomic emission spectrometry and electrochemical sensing [26–28]. However, these methods require expensive equipment, time-consuming and laborious procedures carried out only by highly trained professionals. Alternatively, fluorescence detections are very popular because fluorescence measurements are very sensitive, easy to perform, and inexpensive [29–32]. Furthermore, the photophysical properties of a

✉ Vladimir B. Bojinov
vlbojin@uctm.edu

[1] Department of Organic Synthesis, University of Chemical Technology and Metallurgy, 8 Kliment Ohridsky Bulv., 1756 Sofia, Bulgaria

[2] Department of Chemistry, Faculty of Science, Assiut University, Assiut, Egypt

fluorophore can be easily tuned using a range of mechanisms: charge, electron and energy transfer, the influence of metal ions, and the destabilization of non-emissive n-π* excited states [33–38].

Since the first introduction of molecular scale logic gates using fluorescent chemosensors, many scientists have focused on designing molecules able to mimic the modern semiconductor based devices to miniaturize the device size to nanoscale [39–41]. The research has extended from simple molecular switches to more complex ones which are capable of executing variety of logic operations including half-adder [42, 43], full-adder [44], keypad lock [45], half-subtractor [46], full-subtractor [44], encoder-decoder [47] and digital comparator [48–51]. Moreover, smart oligonucleotide-based automatons that can play games such as Tic-Tac-Toe have been reported [52]. Such logic operations are of valuable interest for applications such as object coding, intelligent materials, drug delivery and activation, diagnostics or actuation [53, 54].

To the best of our knowledge, several molecular probes for testing and distinguishing between several analysts have been reported [55–61]. To detect only the presence of Cu^{2+} by absorption outcome a Rhodamine 6G/2-hydroxybenzylideneamino conjugate was reported [62]. Herein, we reported on the ability of this probe (Scheme 1) to detect several analytes, including H^+, HO^-, Cu^{2+}, Hg^{2+}, Fe^{3+}, Co^{2+}, Cd^{2+}, Zn^{2+}, Sn^{2+}, Ni^{2+}, Al^{3+}, Pb^{2+}, $Ce^{3+}$and Ag^+, by unambiguously colorimetric and fluorimetric outcomes.

Experimental

Materials

Probe **3** was synthesized according to the reported procedure [62]. Rhodamine 6G, hydrazine monohydrate and 2-hydroxybenzaldehyde (Aldrich materials) were used as purchased. Used solvents (Aldrich, Fisher Chemical) were pure or of spectroscopy grade. $Zn(NO_3)_2$, $Cu(NO_3)_2$, $Ni(NO_3)_2$, $Co(NO_3)_2$, $Pb(NO_3)_2$, $Fe(NO_3)_3$, $Hg(NO_3)_2$, $Al(NO_3)_3$, $Cd(NO_3)_2$, $AgNO_3$, $CeCl_3$ and $SnCl_2$ salts were the sources for metal cations (all Aldrich salts at p.a. grade).

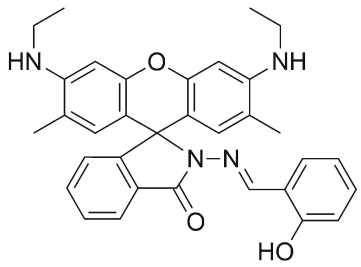

Rhodamine 6G - 2-hydroxybenzylideneamino

(3)

Scheme 1 Rhodamine 6G based probe **3**

Methods

FT-IR spectra were recorded on a Varian Scimitar 1000 spectrometer. The NMR spectra (chemical shifts are given as δ in ppm) were recorded on a Bruker DRX-250 spectrometer operating at 250.13 MHz. The UV-VIS absorption spectra were recorded on a spectrophotometer Hewlett Packard 8452A. The fluorescence spectra were taken on a Scinco FS-2 spectrofluorimeter. All the experiments were performed at room temperature (25.0°C). For all spectroscopic analysis a 1 × 1 cm quartz cuvette are used. To adjust the pH, very small volumes of hydrochloric acid and sodium hydroxide are used. The effect of the metal cations upon the fluorescence intensity was examined by adding portions of the metal cations stock solution to a known volume of the fluorophore solution (3 mL). The addition was limited to 100 μL so that dilution remains insignificant.

Synthesis

Synthesis of Rhodamine 6G hydrazide (2)

To a solution of Rhodamine 6G **1** (2.4 g, 5 mmol) in 40 mL of absolute ethyl alcohol, 1.46 mL of hydrazine monohydrate (30 mmol, $d = 1.032$) was added dropwise at room temperature over a period of 30 min. The resulting solution was stirred at reflux for 5 h. After cooling to room temperature the solid precipitated was filtered off, washed with water and dried to give 1.91 g (89%) of **2** as pale pink crystals ($R_f = 0.57$ in a solvent system toluene/ethylacetate/ethanol = 10:2.5:1). IR (KBr) cm^{-1}: 3280, 3204 (νNH and νNH_2); 2920, 2810 (νCH); 1662 (νC=O); 1600, 1568 and 1496 (νArCH=). ^1H NMR ($CDCl_3$-*d*, 250.13 MHz) ppm: 7.96 (m, 1H, 9-Ph H-3); 7.45 (m, 2H, 9-Ph H-4 and 9-Ph H-5); 7.06 (m, 1H, 9-Ph H-6); 6.39 (s, 2H, Rhodamine H-4 and H-5); 6.26 (s, 2H, Rhodamine H-1 and H-8); 3.58 (s, 2H, NH_2); 3.52 (br.s, 2H, 2 x NH); 3.21(q, 4H, $J = 3.5$ Hz, 2 x $\underline{CH_2}CH_3$); 1.92 (s, 6H, 2 x Ar-CH_3); 1.32 (t, 6H, $J = 7.1$ Hz, 2 x $CH_2\underline{CH_3}$). Elemental analysis: Calculated for $C_{26}H_{28}N_4O_2$ (MW 428.53) C 72.87, H 6.59, N 13.07%; Found C 73.23, H 6.38, N 12.82%.

Synthesis of probe 3

To a solution of Rhodamine 6G hydrazide **2** (1.92 g, 4.5 mmol) in 120 mL of ethanol/dichloromethane (1:3, *v*/v), 5 equivalents of salicylic aldehyde (2.75 g, 22.5 mmol) was added. After the addition, the mixture refluxed in an oil bath with stirring for 12 h. Then the solvent was removed in vacuum. The residue was washed by ethanol (5 × 30 mL) and dried to

afford 2.06 g (86%) of probe **3** (m.p. 288-90 °C; $R_f = 0.89$ in petroleum ether:ethyl acetate = 1:2). IR (KBr) cm^{-1}: 3342 (νOH); 3264 (νNH); 2916, 2804 (νCH); 1666 (νC=O); 1598, 1564 and 1502 (νArCH=). ^1H NMR ($CDCl_3$-*d*, 250.13 MHz) ppm: 10.78 (s, 1H, OH); 9.08 (s, 1H, N=CH); 7.98 (m, 1H, 9-Ph H-3); 7.48 (m, 2H, 9-Ph H-4 and 9-Ph H-5); 7.10 (m, 1H, 9-Ph H-6); 7.02 (m, 1H, Ph-H); 6.94 (d, 1H, J = 5.8 Hz, Ph-H); 6.80 (d, 1H, J = 6.0 Hz, Ph-H); 6.69 (dd, 1H, J = 5.8 Hz, J = 6.0 Hz, Ph-H); 6.40 (s, 2H, Rhodamine H-4 and H-5); 6.29 (s, 2H, Rhodamine H-1 and H-8); 3.46 (br.s, 2H, 2 × NH); 3.19 (q, 4H, J = 3.6 Hz, 2 × $\underline{CH_2}CH_3$); 1.91 (s, 6H, 2 × Ar-CH_3); 1.30 (t, 6H, J = 7.1 Hz, 2 × $CH_2\underline{CH_3}$). Elemental analysis: Calculated for $C_{33}H_{32}N_4O_3$ (MW 532.63) C 74.41, H 6.06, N 10.52%; Found C 74.16, H 5.98, N 10.71%.

Results and discussion

Synthesis of the intermediate Rhodamine 6G hydrazide (2)

The intermediate Rhodamine 6G hydrazide (**2**) was prepared as we described before (Scheme 2) after condensation of Rhodamine 6G with hydrazine monohydrate [10, 63].

Synthesis of the probe Rhodamine 6G - 2-hydroxybenzylideneamino (3)

Probe **3** was synthesized by conversion of intermediate **2** into the desired Rhodamine 6G - 2-hydroxybenzylideneamino conjugate (**3**) by reaction with 2-hydroxybenzaldehyde in ethanol/dichloromethane medium (Scheme 3).

Influence of pH on the photophysical characteristics of probe 3

The photophysical characteristics of the probe were examined in water/DMF (1:4, *v*/v) solution. We began the pH titration from low pH to assert the presence of rhodamine in the fluorescent ring-opening form. As is shown in Fig. 1, at the start of the titration (pH 1.79), the probe exhibited three absorption bands. They are centered at: (i) 534 nm ($\varepsilon = 8.1 \times 10^4$ $L{\cdot}mol^{-1}{\cdot}cm^{-1}$), that is characteristic of the rhodamine moiety in the ring-opening form; (ii) 340 nm ($\varepsilon = 1.8 \times 10^4$ $L{\cdot}mol^{-1}{\cdot}cm^{-1}$) that is characteristic of the 2-hydroxyphenyl hydrazone moiety (the benzenoid form); (iii) 295 nm ($\varepsilon = 3 \times 10^4$ $L{\cdot}mol^{-1}{\cdot}cm^{-1}$) caused by the rhodamine moiety.

By increasing the pH, the absorption at 534 nm was decreasing sharply until pH ≈ 5 and then became nearly constant ($\varepsilon = 7 \times 10^3$ $L{\cdot}mol^{-1}{\cdot}cm^{-1}$) unaffected by further increasing in the pH. This phenomenon is attributed to the conversion of rhodamine moiety from the ring-opening form to the spirolactam form (Scheme 4R1). In the same time, in increasing the pH, the absorption centered at 340 nm shifted to 386 nm with an isosbestic point at 360 nm. This shift was well pronounced after pH = 8 and attributed to the conversion of the 2-hydroxyphenyl hydrazone moiety from the benzenoid form (340 nm) to the induced by OH deprotonation quinoid form (386 nm).

From the absorption changes at 534 nm and 386 nm, the titration curves were obtained Fig. 1 (Insets A and B). The analysis of the titration curves according to Eq. (1) gave the pK_a values of 9.92 and 3.64 corresponding to the conversion of the 2-hydroxyphenyl hydrazone moiety (from benzenoid to quinoid form) and the rhodamine moiety (from ring-opened to ring-closed form), respectively (Table 1).

$$pH = pK_a + \log\frac{(I_{max} - I)}{I - I_{min}} \quad (1)$$

Where I_{max} and I_{min} are the maximum and minimum absorbance, respectively, and I is the absorbance at the corresponding pH value.

On the other hand, as is illustrated in Fig. 2a, at pH ≈ 1.8 after excitation at 510 nm, the probe exhibited an emission centered at 560 nm attributed to the fluorescent ring-opened form of the rhodamine moiety. With the increasing of pH the fluorescence intensity decreased significantly and reached the

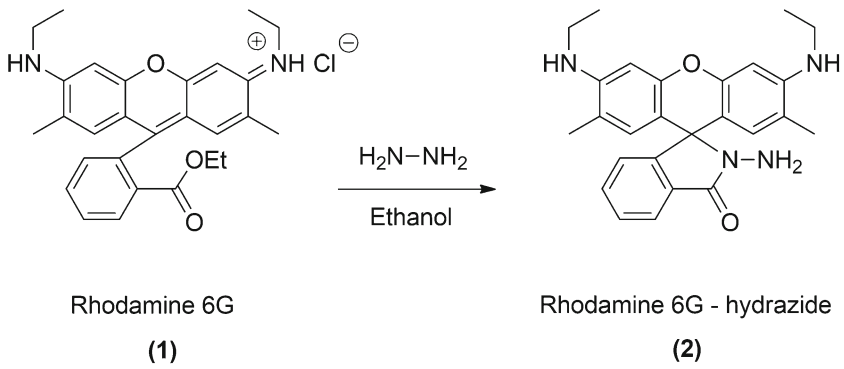

Scheme 2 Synthesis of the intermediate Rhodamine 6G hydrazide (**2**)

Scheme 3 Synthesis of Rhodamine 6G/2-hydroxybenzylideneamino based probe **3**

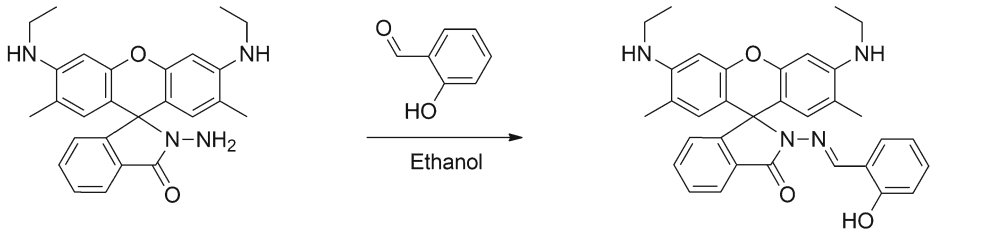

Rhodamine 6G - hydrazide **(2)**

Rhodamine 6G - 2-hydroxybenzylideneamino **(3)**

minimum at pH ≈ 5, then became constant unaffected by further increasing the pH. After excitation at 400 nm (Fig. 2b) the probe exhibited emission centered at 560 nm (pH ≈ 1.8) ascribed to the ring-opened form of the rhodamine moiety. With the increasing of pH, the fluorescence emission at 560 nm decreased and reached the minimum at near pH ≈ 5. In the same time, there was an emission at 510 nm appeared after pH ≈ 8 that was increasing by increasing pH.

From the titration plot of the fluorescence emission at 560 nm, after excitation at 510 nm, against pH (Inset of Fig. 2a) and according to Eq. (2), the pK_a value of the rhodamine conversion from the ring-opened to spirolactam form is 3.44 (Table 1). For the fluorescence emission at 560 nm, after excitation at 400 nm, the same pK_a value (3.44) was obtained (Inset of Fig. 2b).

$$pH = pK_a + \log\frac{(F_{max}-F)}{F-F_{min}} \quad (2)$$

Where F_{max} and F_{min} are the maximum and minimum fluorescence intensity, respectively, and F is the fluorescence intensity at the corresponding pH value.

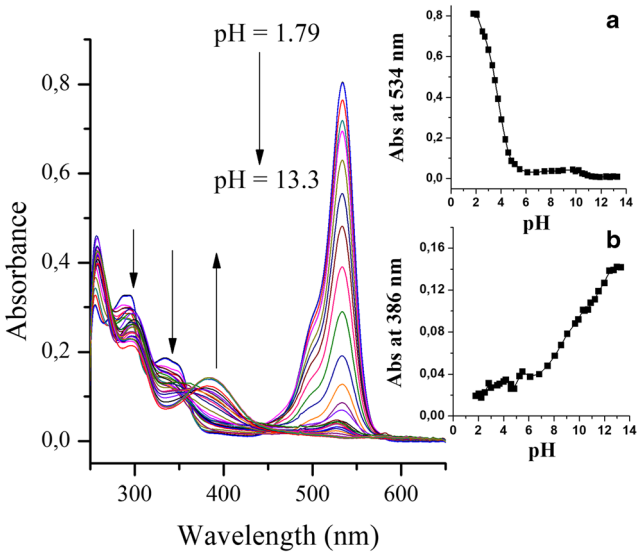

Fig. 1 Effect of pH on the absorption spectrum of probe **3** (C = 10^{-5} mol L^{-1}, DMF:distilled water =1:4, *v*/v). Insets **a** and **b** represents the absorbance at 534 nm and 386 nm, respectively

Similarly, the pK_a value of the conversion of 2-hydroxyphenyl hydrazone (from the benzenoid to quinoid form) was found to be 9.64 (Table 1) using the titration plot of the fluorescence emission at 510 nm, after the excitation at 400 nm (Inset of Fig. 2b).

Influence of cations on the photophysical characteristics of probe 3

The signal-reporting properties of the rhodamine 6G/salicylaldehyde hydrazone conjugate have been reported regarding the selectivity to Cu^{2+} in ethanol:water (1: 1, v / v), however, only in an absorption mode [62]. Many features make fluorescence one of the most powerful transduction mechanisms to report the chemical recognition event. In the fluorescence technique, the sensitivity is high that allow even the detection of single molecules. It is possible to perform remote monitoring, different assays can be designed based on different aspects of the fluorescence output (lifetime, intensity, anisotropy and energy transfer), and additionally, laser fiber optics and detection technologies are well-established [64–68]. So that, in the present work, we investigated the sensory behavior of probe **3** in pure organic solvent, such as DMF, where the probe can work by fluorescence mechanism detecting cations.

The signaling fluorescent properties of probe **3** toward wide range of representative metal ions (Cu^{2+}, Hg^{2+}, Fe^{3+}, Co^{2+}, Cd^{2+}, Zn^{2+}, Sn^{2+}, Ni^{2+}, Ce^{3+}, Al^{3}, Ag^{+} and Pb^{2+}) were studied in DMF. To provide a neutral environment in which the 2-hydroxyphenyl hydrazone and rhodamine units in probe **3** are in their "off state" and the cation recognition by both moieties will not be feasible under such conditions, experiments were conducted in buffered solutions (1 mmol HEPES, pH = 7.2).

As is shown in Fig. 3, several cations including Cu^{2+}, Hg^{2+}, Co^{2+}, Zn^{2+} and Fe^{3+} affected significantly the absorption spectrum of the probe in DMF. The presence of Cu^{2+} led to appearance of two absorption bands centered at 534 nm ($\varepsilon = 4.7 \times 10^4$ L·mol^{-1}·cm^{-1}) and at 412 nm ($\varepsilon = 2.1 \times 10^4$ L·mol^{-1}·cm^{-1}).

The effect of Cu^{2+} is due to the coordination of the metal ion with the 2-hydroxyphenyl hydrazone moiety of the probe

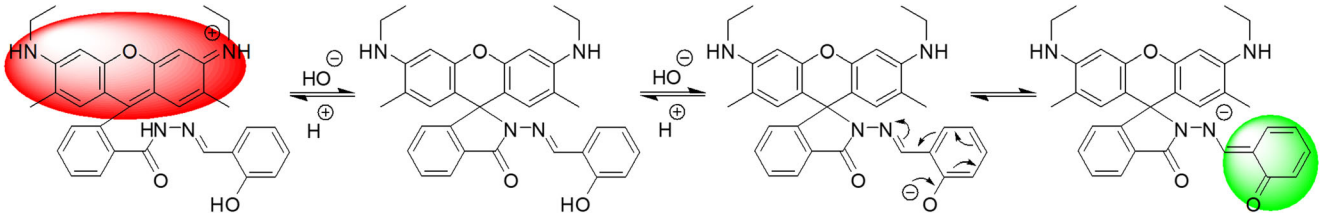

Scheme 4 Transformation of probe **3** as a function of pH

that induces its conversion to the responsible for the absorption band at 412 nm quinoid form. Transforming of the 2-hydroxyphenyl unit from a benzenoid of a quinoid form provokes intramolecular protonation of the rhodamine moiety that induces its conversion to the ring-opened form, responsible for the absorption band at 534 nm (Scheme 5R1).

Surprisingly, Hg^{2+} and Fe^{3+} caused only the appearance of absorption bands centered at 534 nm ($\varepsilon = 1.6 \times 10^4$ L·mol^{-1}·cm^{-1}) and 532 nm ($\varepsilon = 7 \times 10^3$ L·mol^{-1}·cm^{-1}), respectively. The effect by Hg^{2+} and Fe^{3+} can be ascribed to the coordination of these cations with the probe inducing only the ring-opening of the rhodamine moiety [69–71]. Contrariwise, Co^{2+} and Zn^{2+}caused the appearance of only one new absorption band centered at 412 nm ($\varepsilon = 5.5 \times 10^3$ L·mol^{-1}·cm^{-1}) because of the coordination with 2-hydroxyphenyl hydrazone moiety, thus inducing only its conversion to quinoid form without opening of the rhodamine moiety.

Emission spectrum of probe **3** exhibited a week fluorescence emission at 535 nm due to the partial conversion of 2-hydroxyphenyl hydrazone moiety to quinoid form induced by DMF molecules. Among the tested metal ions, after excitation at 510 nm only Hg^{2+} affected vastly the probe fluorescence spectrum) Fig. 4a). Hg^{2+} enhanced the fluorescence emission at 560 nm by 9520%. In contrast, after excitation at 400 nm, the emission spectrum was affected significantly by most of the cations, including Hg^{2+}, Sn^{2+}, Fe^{3+}, Cu^{2+}, Co^{2+},Ni^{2+}, $Cd^{2+}$and Zn^{2+} (Fig. 4b).

Hg^{2+} Sn^{2+} and Fe^{3+} blue-shifted the fluorescence emission at 535 nm to 515 nm decreasing it by 56%, 59% and 18%, respectively. Concomitantly a new emission at 560 nm appeared because of energy transfer from 2-hydroxyphenyl hydrazone moiety to rhodamine moiety after the coordination of metal ions with rhodamine moiety thus inducing conversion of the latter to its fluorescent form that absorption spectrum confirmed. The fluorescence emission at 560 nm observed in the case of Hg^{2+} was the highest and due to the

Table 1 pK_a values of the different conversions of probe **3** because of the pH change

	Absorbance		Emission	
	534 nm	386 nm	510 nm (λ_{ex} 400 nm)	560 nm (λ_{ex} 510 nm)
Rhodamine conversion	3.64	–	3.44	3.44
Salicylaldehyde conversion	–	9.92	9.64	–

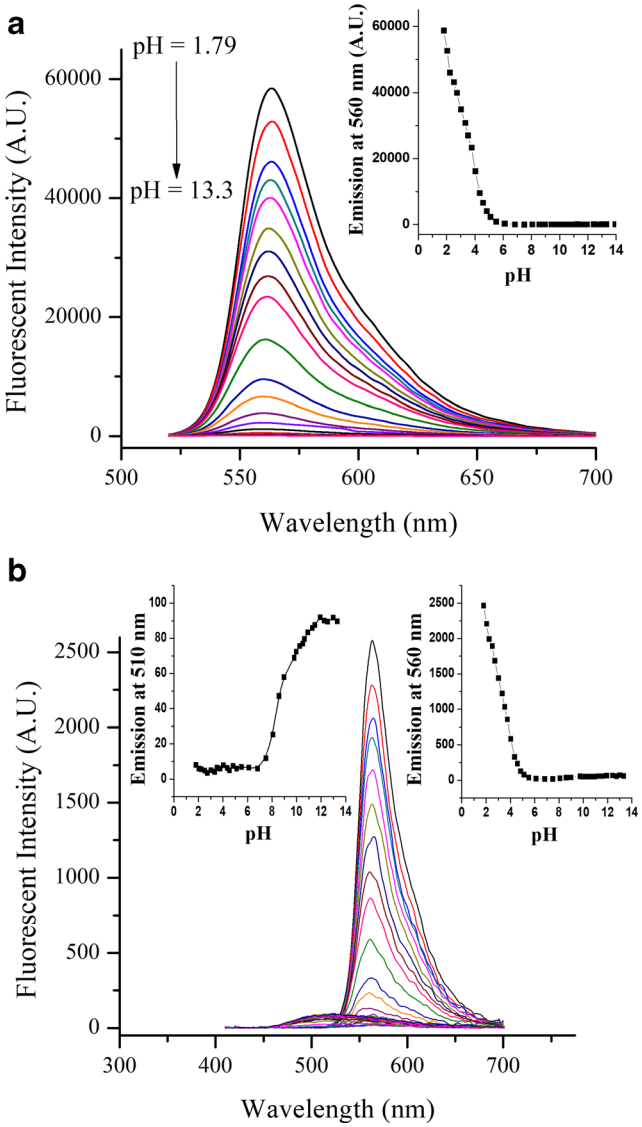

Fig. 2 Effect of pH on the fluorescence emission of probe **3** (C = 10^{-5} mol L^{-1}, DMF:distilled water =1:4, v/v) after excitation at **a** 510 nm and **b** 400 nm. Inset of Fig. 2a: Titration plot of the emission at 560 nm. Insets of Fig. 2b: Titration plots of the emissions at 560 nm and 510 nm

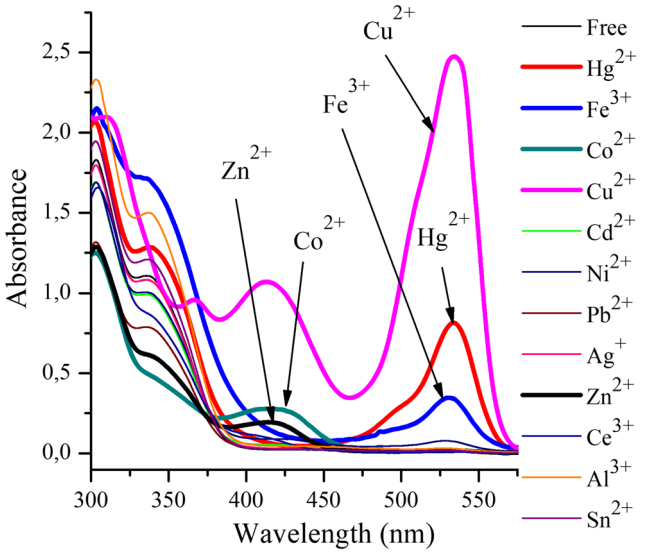

Fig. 3 Effect of metal cations (five equivalent, C = 2.5 × 10^{-4} mol L^{-1}) on the absorption spectrum of probe **3** in DMF solution

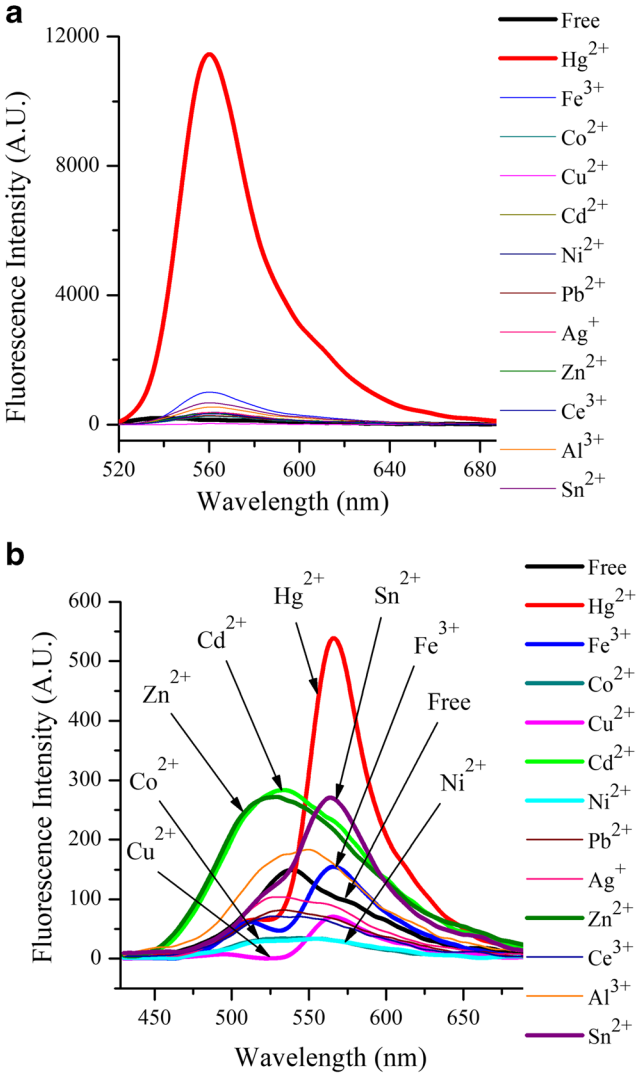

Fig. 4 Effect of cations (five equivalent, C = 2. 5 × 10^{-4} mol L^{-1}, DMF) on the emission spectrum of probe **3** (C = 5 × 10^{-5} mol L^{-1}, DMF) after the excitation **a** at 510 nm and **b** at 400 nm

two factors: (i) the strongest coordination between rhodamine and Hg^{2+} as was confirmed by the highest rhodamine absorption of the complex, and (ii) the paramagnetic properties of Fe^{3+} and Sn^{2+} that cause unspecific fluorescence quenching by energy or electron transfer [72]. Sn^{2+} detection was discriminative by its higher relative quantum yield that is 16.8 times higher than Hg^{2+} and 25.4 times higher than Fe^{3+}. The observed fluorescence emission at 560 nm, although there was no absorption at 530 nm, in the case of Sn^{2+} means that the coordination was in the excited state and not in the ground state [73–76].

Due to their paramagnetic properties Cu^{2+}, Co^{2+} and Ni^{2+} exhibited discriminative effect quenching the emission of 2-hydroxyphenyl hydrazine unit [72, 77]. Zn^{2+} and Cd^{2+} caused only enhancement of the fluorescence emission of 2-hydroxyphenyl hydrazone moiety. However, the quantum yield in the case of Cd^{2+} was 3.6 times higher than that of Zn^{2+}. This means that the coordination between Cd^{2+} and the quinoid form of 2-hydroxyphenyl hydrazone was more efficient in the excited state than in the ground state.

The interesting absorption and emission behavior of probe **3** in the presence of Hg^{2+} was a reason to investigate the interfering influence of a wide range of representative metal ions. Figure 5a illustrates the influence of the interfering cations on the absorption response by the probe towards Hg^{2+}. As can be seen, except Cu^{2+} and Fe^{3+}, all cations under study decreased absorbance at 534 nm. The most obvious decrease in the absorbance of the probe at 534 nm was recorded in the

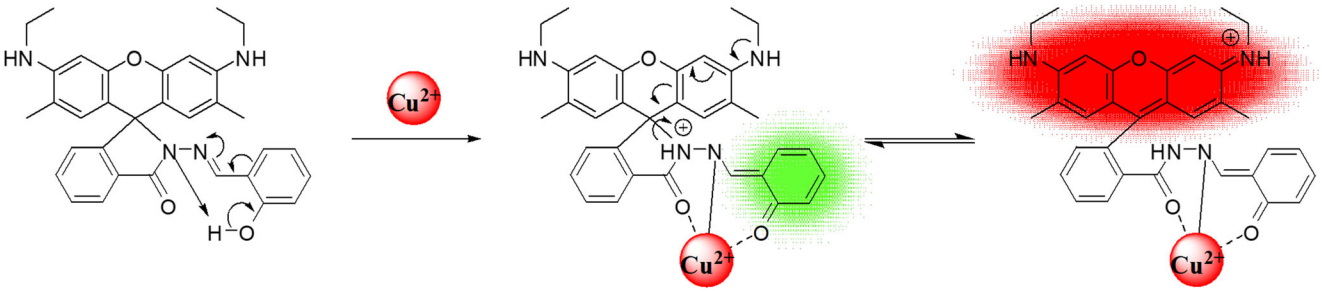

Scheme 5 Conversion of probe **3** provoked by Cu^{2+}

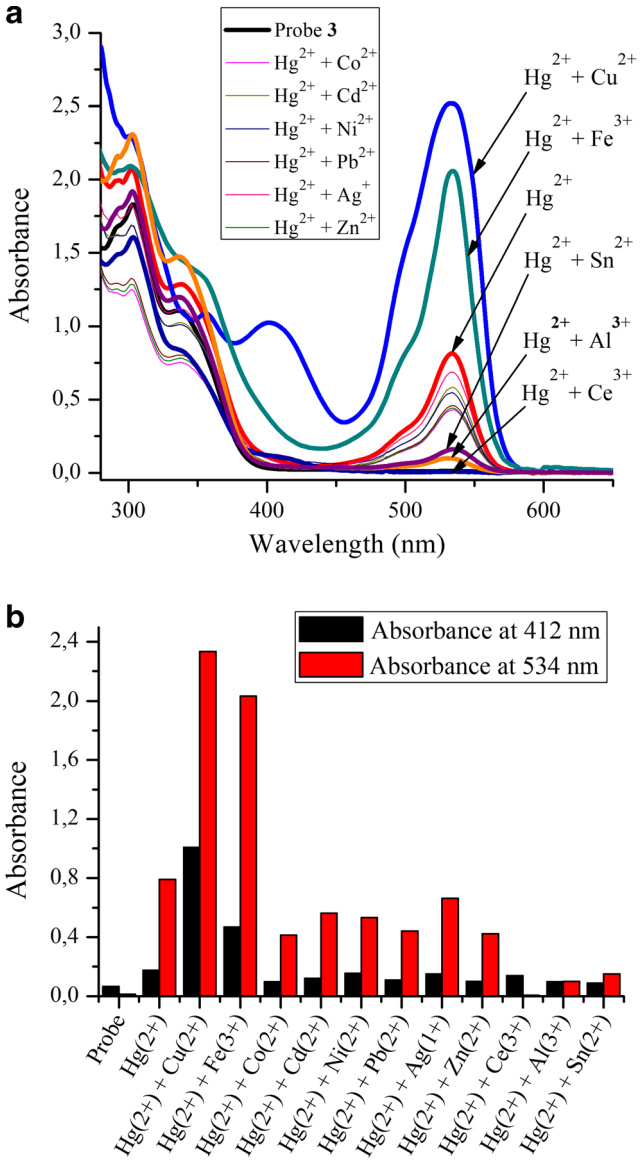

Fig. 5 Effect of interfering cations (five equivalent, C = 2.5 × 10^{-4} mol L^{-1}, DMF) on the **a** absorption spectrum and **b** absorbance at 534 nm and 412 nm of probe **3** (C = 5 × 10^{-5} mol L^{-1}, DMF) respond towards Hg^{2+} (five equivalent, C = 2.5 × 10^{-4} mol L^{-1}, DMF)

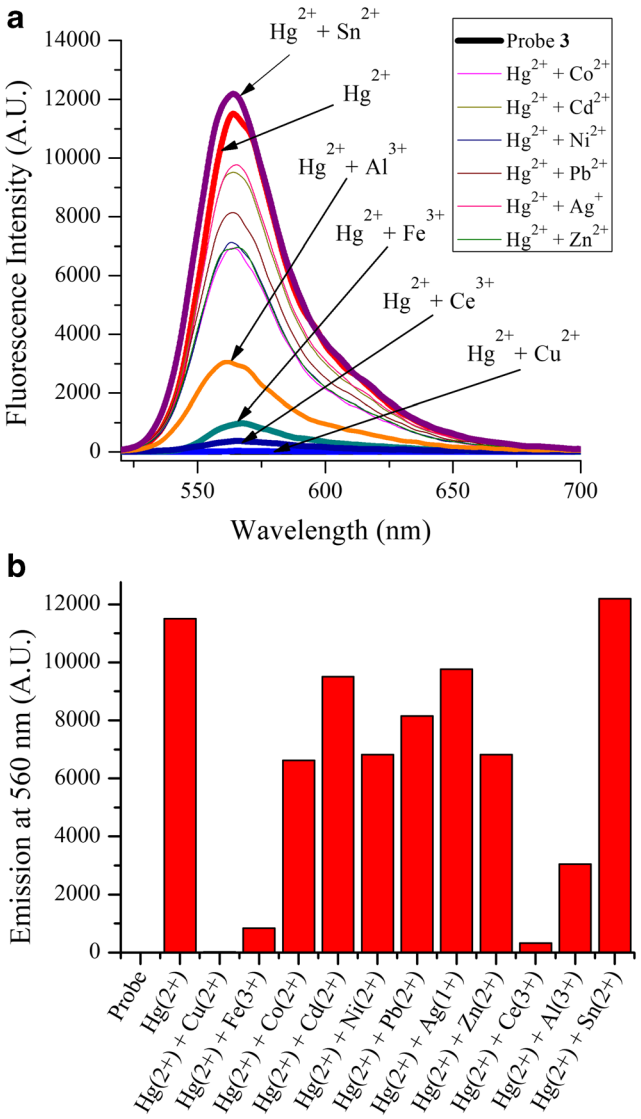

Fig. 6 Effect of interfering cations (five equivalent, C = 2.5 × 10^{-4} mol L^{-1}, DMF) on **a** fluorescence emission spectrum and **b** fluorescence emission at 560 nm after the excitation at 510 nm of probe **3** (C = 5 × 10^{-5} mol L^{-1}, DMF) respond towards Hg^{2+} (five equivalent, C = 2.5 × 10^{-4} mol L^{-1}, DMF)

presence of Ce^{3+} (99%), Al^{3+} (87%) and Sn^{2+} (81%). The competition of the interfering metal ions with Hg^{2+} and their ability to replace the latter from its complex with the probe ascribes the decrease of the absorbance. As a result, these cations induced neither the ring-opening of rhodamine nor the conversion of salicylaldehyde hydrazone to the quinoid form. Also, as it is clear from Fig. 5, the presence of Cu^{2+} increased the absorbance at 534 nm in addition to the appearance of a new absorption band centered at 412 nm ($\varepsilon = 2 \times 10^4$ $L{\cdot}mol^{-1}{\cdot}cm^{-1}$). However, the presence of Fe^{3+} only enhanced vastly the absorbance at 534 nm. The effect by Cu^{2+} and Fe^{3+} is due to their ability to replace Hg^{2+} from its complex with the probe. In addition, while Cu^{2+} is able to induce the both ring-opening of rhodamine and conversion of 2-hydroxyphenyl hydrazone to the quinoid form, Fe^{3+} is only capable of inducing the ring-opening of rhodamine.

Figure 6 demonstrates the influence of the interfering cations on the response of the probe towards Hg^{2+} in a fluorescence mode. All the interfering cations under study, except Sn^{2+}, quenched the fluorescence emission at 560 nm after the excitation at 510 nm. The most obvious quenching was by Cu^{2+} (99.9%), Ce^{3+} (97%), Fe^{3+} (92%) and Al^{3+} (72%). These cations replaced Hg^{2+} from its complex with the probe, which was accompanied with the quenching of the fluorescence emission.

The presence of Sn^{2+} not only increased the fluorescence emission of rhodamine moiety but also increased its quantum

Table 2 Scheme for detecting of cations by probe **3** in DMF

Analyte	Absorption		Emission		
	A 412 nm	A 534 nm	Excitation at 400 nm		Excitation at 510 nm
			F 535 nm	F 560 nm	F 560 nm
Cu^{2+}	↑	↑	↓	↓	
Hg^{2+}		↑	↓	↑	↑
Fe^{3+}		↑	↓	↑	↑
Co^{2+}	↑		↓	↓	
Cd^{2+}			↑	↑	
Zn^{2+}	↑		↑	↑	
Sn^{2+}				↑	↑
Ni^{2+}		↑	↓	↓	

↑ and ↓ demonstrate increase and decrease in the signal, respectively

yield. Using Eq. (3), the ratio between the quantum yield of fluorescence emission by rhodamine moiety in the presence of Hg^{2+} before (Φ_1) and after (Φ_2) addition of Sn^{2+} can be calculated from ($\Phi_2/\Phi_1 = S_2/S_1 \times A_1/A_2$). A_1 and A_2 are the absorbance at 534 nm before and after the addition of Sn^{2+}, respectively, and S_1 and S_2 are the integrated band area of the emission at 560 nm before and after the addition of Sn^{2+}, respectively. The calculated value of 5.7 for Φ_2/Φ_1 means that the quantum yield of the probe–Hg^{2+} complex increased practically six times by adding Sn^{2+}.

$$\phi_F = \phi_{ref.}\left(\frac{S_{sample}}{S_{ref}}\right)\left(\frac{A_{ref.}}{A_{sample}}\right)\left(\frac{\eta^2_{sample}}{\eta^2_{ref.}}\right) \quad (3)$$

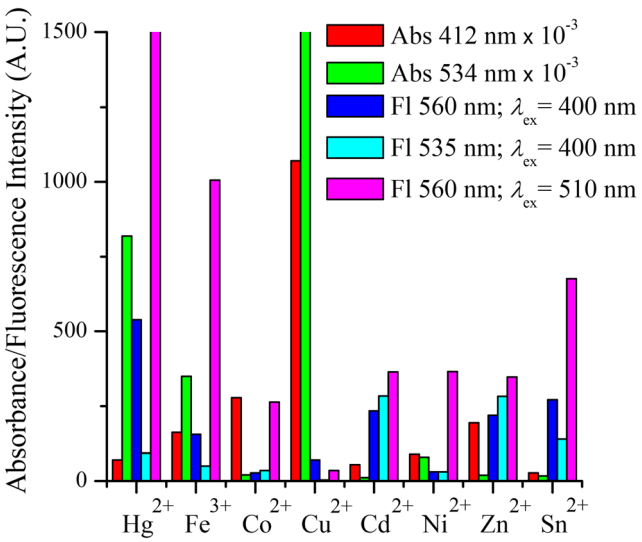

Fig. 7 The unique effect of Cu^{2+}, Hg^{2+}, Fe^{3+}, Co^{2+}, Cd^{2+}, Zn^{2+}, Sn^{2+} and Ni^{2+} on the probes **3** signaling properties which could be recognized as a fingerprint of each analyte

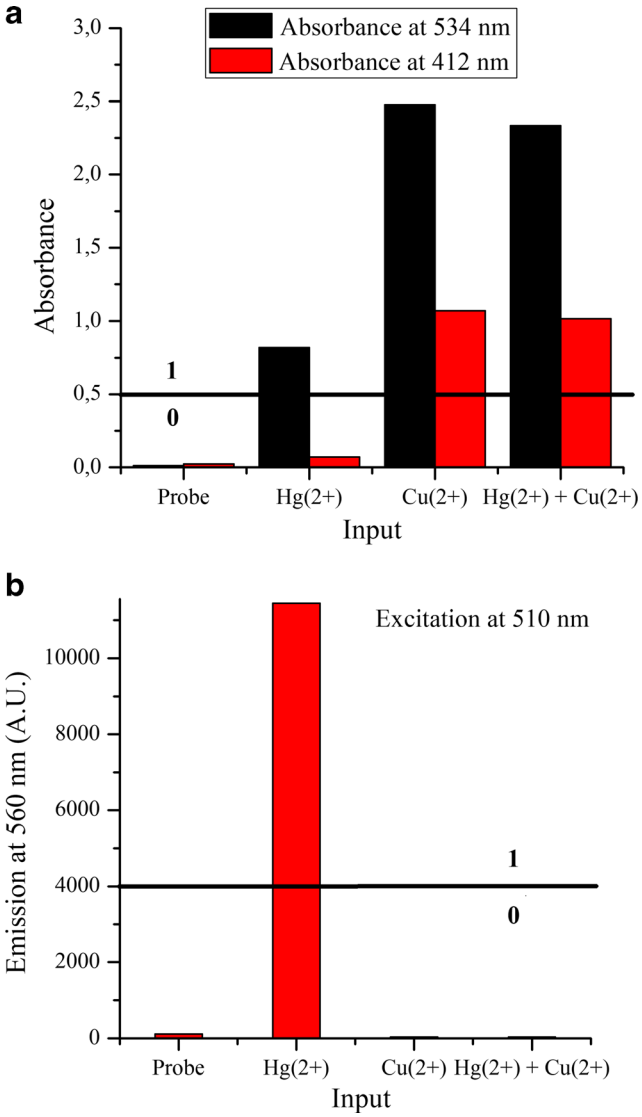

Fig. 8 The changes in the **a** absorbance at 534 nm and 412 nm and **b** emission at 560 nm ($\lambda_{ex.} = 510$ nm) of the probe ($C = 5 \times 10^{-5}$ mol L^{-1}) in the presence of Cu^{2+} ($C = 2.5 \times 10^{-4}$ mol L^{-1}) and Hg^{2+} ($C = 2.5 \times 10^{-4}$ mol L^{-1}) as chemical inputs

Where, $\Phi_{ref.}$ is the quantum yield of the reference compound, $A_{ref.}$, $S_{ref.}$, $\eta_{ref.}$ and A_{sample}, S_{sample}, η_{sample}, represent the absorbance at the exited wavelength, the integrated emission band

Table 3 The truth table for logic behavior of probe **3** using Hg^{2+} and Cu^{2+} as inputs

Input 1	Input 2	Output 1	Output 2	Output 3
Cu^{2+}	Hg^{2+}	$A_{534\ nm}$	$A_{412\ nm}$	$F_{560\ nm}$
0	0	0	0	0
0	1	1	0	1
1	0	1	1	0
1	1	1	1	0
Logic Gate:		*OR*	*TRANSFER* (Cu^{2+})	*INHIBIT* (Hg^{2+})

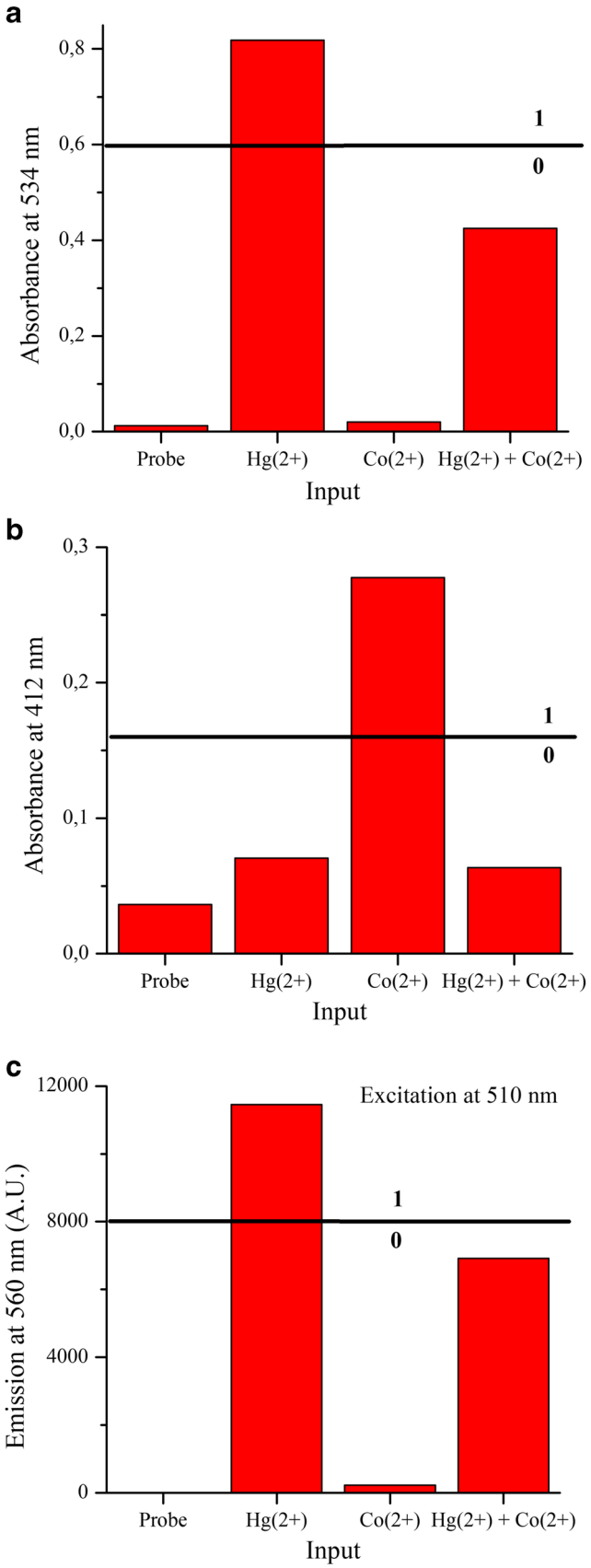

◀ **Fig. 9** The changes in the **a** absorbance at 534 nm, **b** absorbance at 412 nm and **c** emission at 560 nm ($\lambda_{ex.} = 510$ nm) of probe **3** ($C = 5 \times 10^{-5}$ mol L^{-1}) in the presence of Co^{2+} ($C = 2.5 \times 10^{-4}$ mol L^{-1}) and Hg^{2+} ($C = 2.5 \times 10^{-4}$ mol L^{-1}) as chemical inputs

area and the solvent refractive index of the reference and the sample, respectively.

After excitation at 400 nm, the interfering cations exhibited influence similar to that observed after excitation at 510 nm, as the Sn^{2+} ion enhanced the fluorescence emission even more. The observed effect of Sn^{2+} as an interfering cation is due to its displacement of Hg^{2+} from its complex and as we mentioned above, Sn^{2+} coordinates with the probe in the excited state inducing the conversion of both 2-hydroxyphenyl and rhodamine moieties into their fluorescent forms.

From above, the present probe **3** could discriminatively to detect several cations. The increase of the absorptions in aqueous solutions means that the present analyte is Cu^{2+}. The other cations can be detected in DMF: the increase in the absorption at 534 nm and the emission at 560 nm after excitation at 510 nm means that the analyte is Hg^{2+}; the increase of the absorption at 534 nm and the fluorescence intensity at 560 nm ($\lambda_{ex.} = 400$ nm and $\lambda_{ex.} = 510$ nm) means the analyte is Fe^{3+}; the increase in the fluorescence emission at 535 nm ($\lambda_{ex.} = 400$ nm) with increase in the absorption at 412 nm means the analyte is Zn^{2+}, but when there is no increase in the absorption means that the analyte is Cd^{2+}; the fluorescence quenching at 535 nm ($\lambda_{ex.} = 400$ nm) means the analye is Ni^{2+}; the emission enhancement at 560 nm ($\lambda_{ex.} = 400$ nm) without increase in the absorption at 534 nm means the analyte is Sn^{2+} (Table 2).

In fact, the presented in Table 2 results reveal that probe **3** works like an artificial tongue at molecular level. In the artificial tongues, there is no need for selective interactions between the probe and analytes. In these systems, the different analytes give rise to unique variety of the probe signal outputs and each analyte could be recognized as a fingerprint for identification [78]. As can been seen from Table 2 and Fig. 7 the presence Cu^{2+}, Hg^{2+}, Fe^{3+}, Co^{2+}, Cd^{2+}, Zn^{2+}, Sn^{2+} or Ni^{2+} leads to unique changes in the five signaling outputs of **3**.

Table 4 The truth table for logic behavior of probe **3** using Hg^{2+} and Co^{2+} as inputs

Input 1	Input 2	Output 1	Output 2	Output 3
Co^{2+}	Hg^{2+}	$A_{534\ nm}$	$A_{412\ nm}$	$F_{560\ nm}$
0	0	0	0	0
0	1	1	0	1
1	0	0	1	0
1	1	0	0	0
Logic Gate:		*INHIBIT* (Hg^{2+})	*INHIBIT* (Co^{2+})	*INHIBIT* (Hg^{2+})

Logic behavior of probe 3

From Fig. 8, firstly, the probe alone ($C = 5 \times 10^{-5}$ mol L^{-1}, DMF) exhibited a low output (coded as binary 0) for the absorptions at 534 nm and 412 nm and the fluorescence emission at 560 nm ($\lambda_{ex.} = 510$ nm). Secondly, the presence of Hg^{2+} as a chemical input ($C = 2.5 \times 10^{-4}$ mol L^{-1}, DMF) gave a high output (coded as binary 1) for the absorbance at 534 nm and the fluorescence emission at 560 nm and a low output for the absorbance at 412 nm. The presence of Cu^{2+} ($C = 2.5 \times 10^{-4}$ mol L^{-1}, DMF) alone led to a high output of the absorptions at 534 nm and 412 nm and a low output for the fluorescence emission at 560. Finally, the presence of Cu^{2+} together with Hg^{2+} quenched the fluorescence emission induced by Hg^{2+} and the fluorescence output became low. However, the absorbance at 534 nm and 412 nm were high outputs. The behavior of the probe at the absorptions of 534 nm and 412 nm as well as the fluorescence emission at 560 nm ($\lambda_{ex.} = 510$ nm) mimics *OR*, *TRANSFER* (Cu^{2+}) and *INHIBIT* (Hg^{2+}) logic gates, respectively, in the presence of Hg^{2+} and Cu^{2+} as inputs in DMF (Table 3).

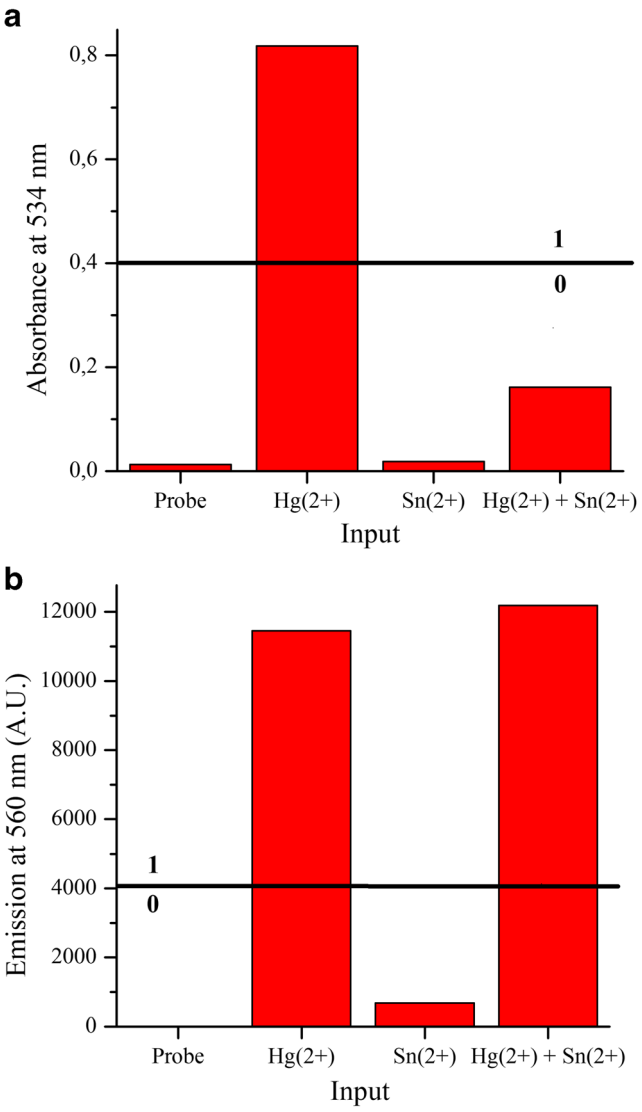

Fig. 10 The changes in the **a** absorbance at 534 nm and **b** emission at 560 nm ($\lambda_{ex.} = 510$ nm) of probe **3** ($C = 5 \times 10^{-5}$ mol L^{-1}) in the presence of Sn^{2+} ($C = 2.5 \times 10^{-4}$ mol L^{-1}) and Hg^{2+} ($C = 2.5 \times 10^{-4}$ mol L^{-1}) as chemical inputs

Table 5 The truth table for logic behavior of probe **3** using Hg^{2+} and Sn^{2+} as inputs

Input 1	Input 2	Output 1	Output 3
Sn^{2+}	Hg^{2+}	$A_{534\ nm}$	$F_{560\ nm}$
0	0	0	0
1	0	0	0
0	1	1	1
1	1	0	1
	Logic Gate:	*INHIBIT* (Hg^{2+})	*TRANSFER* (Hg^{2+})

Figure 9 illustrates absorption behavior of probe **3** at 534 nm and 412 nm as well as emission behavior at 560 nm ($\lambda_{ex.} = 510$ nm) in the presence of all variations of Hg^{2+} and Co^{2+} with the probe. Absorption at 534 nm and emission at 560 nm became high only in the presence of Hg^{2+} alone, while only Co^{2+} alone changed the absorption at 412 nm to high. Described behavior of probe **3** in absorption and emission mode mimics *INHIBIT* logic gates in the presence of Hg^{2+} and Co^{2+} as inputs (Table 4). The system that mimics three *INHIBIT* outputs with two inputs can execute a comparator logic function. The presence of at least one high output means that the two inputs are different and the presence of two high outputs means the presence of a certain input (here is Hg^{2+}).

Figure 10 reflects the behavior of the probes in the presence of Hg^{2+} and/or Sn^{2+}. The absorbance of the probe at 534 nm was high only in the presence of Hg^{2+} alone, but the emission at 560 nm ($\lambda_{ex.} = 510$ nm) became high only in the presence of Hg^{2+}, whether it was alone or was mixed with Sn^{2+}. The absorption (534 nm) and emission (560 nm) behavior of the probe in the presence of Hg^{2+} and Sn^{2+} as chemical inputs mimics *INHIBIT* (Hg^{2+}) and *TRANSFER* (Hg^{2+}) logic gates, respectively (Table 5).

Conclusions

We could here to exploit a single probe (probe **3**) to detect several analysts, including H^+, HO^-, Cu^{2+}, Hg^{2+}, Fe^{3+}, Co^{2+}, Cd^{2+}, Zn^{2+}, Sn^{2+}, Ni^{2+}, Al^{3+}, Pb^{2+}, $Ce^{3+}$and Ag^+, by unambiguously colorimetric and fluorimetric outcomes. In aqueous solutions, probe **3** exhibited different responses at low pH (presence of H^+) and basic pH (presence of HO^-). At low pH, probe **3** exhibited an absorption centered at 534 nm and a fluorescence emission centered at 560 nm, which are characteristic of the ring-opened form of the rhodamine moiety.

However, at high pH the absorption and emission of rhodamine moiety disappeared because of its presence in the non-fluorescent spirolactm form and in the same time, a new absorption centered at 386 nm and fluorescence emission centered at 510 nm ($\lambda_{ex.}$ = 400 nm), which are characterized of the quinoid form of 2-hydroxyphenyl hydrazone moiety. The probe could to distinguish between different cations and to work like an artificial tongue at molecular level. Working in pure DMF probe **3** is able to detect discriminatively several cation, including Cu^{2+}, Hg^{2+}, Fe^{3+}, Co^{2+}, Cd^{2+}, Zn^{2+}, Sn^{2+} and Ni^{2+}, thus providing chemosensoring molecular lab. The different colorimetric and fluorimetric outcomes observed by various cations are due to the different mechanisms of the coordination in addition to the different effects of the various cations on the complex fluorescence emission. Several logic gates including *OR*, *INHIBIT* and *TRANSFER* were performed by the probe. Moreover the probe executed three *INHIBIT* logic gates by two inputs, which was exploited to execute a digital molecular comparator.

Acknowledgements The Science Foundation at the University of Chemical Technology and Metallurgy (Sofia, Bulgaria) supported this work. Authors also acknowledge the Science foundation of Assiut University (Assiut, Egypt).

References

1. Jin W, Jiang J, Wang X, Zhu X, Wang G, Song Y, Bai C (2011) Continuous intra-arterial blood pH monitoring in rabbits with acid-base disorders. Respir Physiol Neurobiol 177:183–188
2. Grant S, Bettencourt K, Krulevitch P, Hamilton J, Glass R (2001) In vitro and in vivo measurements of fiber optic and electrochemical sensors to monitor brain tissue pH. Sensors Actuators B Chem 72:174–719
3. Georgiev N, Said A, Toshkova R, Tzoneva R, Bojinov V (2019) A novel water-soluble perylenetetracarboxylic diimide as a fluorescent pH probe: chemosensing, biocompatibility and cell imaging. Dyes Pigments 160:28–36
4. Young O, Thomson R, Merhtens V, Loeffen M (2014) Industrial application to cattle of a method for the early determination of meat ultimate pH. Meat Sci 67:107–112
5. Zhang X, Jiang H, Jin J, Xu X, Zhang Q (2012) Analysis of acid rain patterns in northeastern China using a decision tree method. Atmos Environ 46:590–596
6. Han J, Burgess K (2011) Fluorescent indicators for intracellular pH. Chem Rev 52:2709–2728
7. Kim N, Swamy KMK, Yoon J (2011) Study on various fluorescein derivatives as pH sensors. Tetrahedron Lett 52:2340–2343
8. Aigner D, Borisov SM, Fernández FJ, Fernández Sánchez JF, Saf R, Klimant I (2012) New fluorescent pH sensors based on covalently linkable PET rhodamines. Talanta 99:194–201
9. Li CY, Zhou Y, Xu F, Li YF, Zou CX, Weng C (2012) A fluorescent pH chemosensor based on functionalized naphthalimide in aqueous solution. Anal Sci 28:743–747
10. Georgiev N, Bryaskova R, Tzoneva R, Ugrinova I, Detrembleur C, Miloshev S, Asiri A, Qusti A, Bojinov V (2013) A novel pH sensitive water soluble fluorescent nanomicellar sensor for potential biomedical applications. Bioorg Med Chem 21:6292–6302
11. Aigner D, Ungerböck B, Mayr T, Saf R, Klimant I, Borisov SM (2013) Fluorescent materials for pH sensing and imaging based on novel 1,4-diketopyrrolo-[3,4-c]pyrrole dyes. J Mater Chem C 1: 5685–5693
12. Dimov S, Georgiev N, Asiri A, Bojinov V (2014) Synthesis and sensor activity of a PET-based 1,8-naphthalimide probe for Zn^{2+} and pH determination. J Fluoresc 24:1621–1628
13. Alamry K, Georgiev N, El-Daly SA, Taib L, Bojinov V (2015) A highly selective ratiometric fluorescent pH probe based on a PAMAM wavelength-shifting bichromophoric system. Spectrochim Acta Part A Mol Biomol Spectrosc 135:792–800
14. Georgiev N, Dimitrova M, Todorova Y, Bojinov V (2016) Synthesis, chemosensing properties and logic behaviour of a novel ratiometric 1,8-naphthalimide probe based on ICT and PET. Dyes Pigments 131:9–17
15. McRae R, Bagchi P, Sumalekshmy S, Fahrni C (2019) In situ imaging of metals in cells and tissues. Chem Rev 109:4780–4827
16. Que EL, Domaille DW, Chang C (2018) Metals in neurobiology: probing their chemistry and biology with molecular imaging. Chem Rev 108:1517–1549
17. Bargossi C, Fiorini MC, Montalti M, Prodi L, Zaccheroni N (2000) Recent developments in transition metal ion detection by luminescent chemosensors. Coord Chem Rev 208:17–32
18. Eisenstein R (2000) Iron regulatory proteins and the molecular control of mammallan iron metabolism. Annu Rev Nutr 20:627–662
19. Tang L, Zhou P, Zhang Q, Huang Z, Zhao J, Cai M (2013) A simple quinoline derivatized thiosemicarbazone as a colorimetic and fluorescent sensor for relay recognition of Cu^{2+} and sulfide in aqueous solution. Inorg Chem Commun 36:100–104
20. Ahamed B, Ghosh P (2011) An integrated system of pyrene and rhodamine-6G for selective colorimetric and fluorometric sensing of mercury(II). Inorg Chim Acta 372:100–107
21. Winder C, Carmichael N, Lewis P (1982) Effects of chronic low level lead exposure on brain development and function. Trends Neurosci 4:207–209
22. Bernardo-Filho M, da Conceicão CM, de Oliveira VJ, Caldeira de Araujo A, Pereira da Silva FC, de Sousa da Fonseca A (1994) Evaluation of potential genotoxity of stannous chloride: inactivation, filamentation and lysogenic induction of Escherichia coli. Food Chem Toxicol 32:477–479
23. Lee HN, Xu ZC, Kim SK, Swamy KMK, Kim Y, Kim SJ, Yoon JY (2007) Pyrophosphate-selective fluorescent chemosensor at physiological pH: formation of a unique excimer upon addition of pyrophosphate. J Am Chem Soc 129:3828–3829
24. Wang JB, Qian XH (2006) Two regioisomeric and exclusively selective Hg(II) sensor molecules composed of a naphthalimide fluorophore and an o-phenylenediamine derived triamide receptor. Chem Commun 2006:109–111
25. Komatsu K, Urano Y, Kojima P, Nagano TJ (2007) Development of an iminocoumarin-based zinc sensor suitable for ratiometric fluorescence imaging of neuronal zinc. J Am Chem Soc 129:13447–13454
26. Butler O, Cook J, Harrington C, Hill S, Rieuwerts J, Miles D (2006) Atomic spectrometry update. Environmental analysis J Anal At Spectrom 21:217–243
27. Li Y, Chen C, Li B, Sun J, Wang J, Gao Y, Zhao Y, Chai Z (2006) Elimination efficiency of different reagents for the memory effect of mercury using ICP-MS. J Anal At Spectrom 21:94–96
28. Leermakers M, Baeyens W, Quevauviller P, Horvat M (2005) Mercury in environmental samples: speciation, artifacts and validation. Trends Anal Chem 24:383–393
29. Georgiev N, Bakov V, Bojinov V (2019) A solid-state-emissive 1,8-naphthalimide probe based on photoinduced electron transfer and aggregation-induced emission. ChemistrySelect 4:4163–4167
30. Czarnik A (1993) Fluorescent chemosensors for ion and molecule recognition. American Chemical Society, Washington

31. Said A, Georgiev N, Bojinov V (2019) A smart chemosensor: discriminative multidetection and various logic operations in aqueous solution at biological pH. Spectrochim Acta Part A Mol Biomol Spectrosc 223:117304
32. Lakowicz J (1983) Principles of fluorescence spectroscopy. Plenum Press, New York
33. Said A, Georgiev N, Bojinov V (2018) Synthesis of a single 1,8-naphthalimide fluorophore as a molecular logic lab for simultaneously detecting of Fe^{3+}, Hg^{2+} and Cu^{2+}. Spectrochim Acta Part A Mol Biomol Spectrosc 196:76–82
34. Goswami S, Sen D, Das N, Hazra G (2010) Highly selective colorimetric fluorescence sensor for Cu2+: cation-induced 'switching on' of fluorescence due to excited state internal charge transfer in the red/near-infrared region of emission spectra. Tetrahedron Lett 51:5563–5566
35. Bojinov V, Panova I, Simeonov D, Georgiev N (2010) Synthesis and sensor activity of photostable blue emitting 1,8-naphthalimides containing s-triazine UV absorber and HALS fragments. J Photochem Photobiol A Chem 210:89–99
36. Kim J, Morozumi T, Kurumatani N, Nakamura H (2008) Novel chemosensor for alkaline earth metal ion based on 9-anthryl aromatic amide using a naphthalene as a TICT control site and intramolecular energy transfer donor. Tetrahedron Lett 49:1984–1987
37. Georgiev N, Sakr A, Bojinov V (2015) Design and synthesis of a novel PET and ICT based 1,8-naphthalimide FRET bichromophore as a four-input disabled-enabled-OR logic gate. Sensors Actuators B Chem 221:625–634
38. Said A, Georgiev N, Bojinov V (2015) Sensor activity and logic behavior of dihydroxyphenyl hydrazone derivative as a chemosensor for Cu^{2+} determination in alkaline aqueous solutions. J Photochem Photobiol A Chem 311:16–24
39. Andréasson J, Pischel U (2010) Smart molecules at work-mimicking advanced logic operations. Chem Soc Rev 39:174–188
40. de Silva AP, McClenaghan N (2004) Molecular-scale logic gates. Chem Eur J 10:574–586
41. Bojinov V, Georgiev N (2011) Molecular sensors and molecular logic gates. J Univ Chem Tech Metall 46:3–26
42. Andréasson J, Straight S, Kodis G, Park CD, Hambourger M, Gervaldo M, Albinsson B, Moore T, Moore A, Gust D (2006) All-photonic molecular half-adder. J Am Chem Soc 128:16259–16265
43. Georgiev N, Lyulev M, Bojinov V (2012) Sensor activity and logic behavior of PET based dihydroimidazonaphthalimide diester. Spectrochim Acta Part A Mol Biomol Spectrosc 97:512–520
44. Margulies D, Melman G, Shanzer A (2006) A molecular full-adder and full-subtractor, an additional step toward a moleculator. J Am Chem Soc 128:4865–4871
45. Li Q, Yue Y, Guo Y, Shao S (2012) Fluoride anions triggered "OFF–ON" fluorescent sensor for hydrogen sulfate anions based on a BODIPY scaffold that works as a molecular keypad lock. Sensors Actuators B Chem 173:797–801
46. Suresh M, Jose D, Das A (2007) [2,2'-Bipyridyl]-3,3′-diol as a molecular half-subtractor. Org Lett 9:441–444
47. Ceroni P, Bergamini G, Balzani V (2009) Old molecules, new concepts: $[Ru(bpy)3]^{2+}$ as a molecular encoder-decoder. Angew Chem Int Ed 48:8516–8518
48. Georgiev N, Lyulev M, Alamry K, El-Daly SA, Taib L, Bojinov V (2014) Synthesis, sensor activity and logic behavior of a highly water-soluble 9,10-dihydro-7H-imidazo[1,2-*b*]benz[*d*,*e*-]isoqionolin-7-one dicarboxylic acid. J Photochem Photobiol A Chem 297:31–38
49. Jiang W, Zhang H, Liu Y (2009) Unimolecular half-adders and half-subtractors based on acid-base reaction. Front Chem China 4: 292–298
50. Georgiev N, Yaneva I, Surleva A, Asiri A, Bojinov V (2013) Synthesis, sensor activity and logic behavior of a highly water-solublenaphthalimide derivative. Sensors Actuators B Chem 184: 54–63
51. Said A, Georgiev N, Bojinov V (2019) A fluorescent bichromophoric "off-on-off" pH probe as a molecular logic device (half-subtractor and digital comparator) operating by controlled PET and ICT processes. Dyes Pigments 162:377–384
52. Macdonald J, Li Y, Sutovic M, Lederman H, Pendri K, Lu W, Andrews B, Stefanovic D, Stojanovic M (2006) Medium scale integration of molecular logic gates in an automaton. Nano Lett 6: 2598–2603
53. Pais V, Remon P, Collado D, Andréasson J, Perez-Inestrosa E, Pischel U (2011) OFF-ON-OFF fluorescence switch with T-latch function. Org Lett 13:5572–5575
54. Pu F, Ju E, Ren J, Qu X (2014) Multiconfigurable logic gates based on fluorescence switching in adaptive coordination polymer nanoparticles. Adv Mater 26:1111–1117
55. Kim YS, Park GJ, Lee JJ, Lee SY, Lee SY, Kim C (2015) Multiple target chemosensor: a fluorescent sensor for Zn(II) and Al(III) and a chromogenic sensor for Fe(II) and Fe(III). RSC Adv 5:11229–11239
56. Alam R, Bhowmick R, Islam ASM, Katarkar A, Chaudhuri K, Ali M (2017) A rhodamine based fluorescent trivalent sensor (Fe^{3+}, Al^{3+}, Cr^{3+}) with potential applications for live cell imaging and combinational logic circuits and memory devices. New J Chem 41:8359–8369
57. Wan X, Liu T, Liu H, Gu L, Yao Y (2014) Cascade OFF-ON-OFF fluorescent probe: dual detection of trivalent ions and phosphate ions. RSC Adv 4:29479–29484
58. Udhayakumari D, Suganya S, Velmathi S, MubarakAli D (2014) Naked eye sensing of toxic metal ions in aqueous medium using thiophene-based ligands and its application in living cells. J Mol Recognit 27:151–159
59. Behera N, Manivannan V (2018) A probe for multi detection of Al^{3+}, Zn^{2+} and Cd^{2+} ions via turn-on fluorescence responses. J Photochem Photobiol A Chem 353:77–85
60. García-Gutiérrez Y, Huerta-Aguilar C, Thangarasu P, Vázquez-Ramos J (2017) Ciprofloxacin as chemosensor for simultaneous recognition of Al^{3+} and Cu^{2+} by logic gates supported fluorescence: application to bio-imaging for living cells. Sensors Actuators B Chem 248:447–459
61. Liu H, Cui S, Shi F, Pu S (2019) A diarylethene based multifunctional sensor for fluorescent detection of Cd^{2+} and colorimetric detection of Cu^{2+}. Dyes Pigments 161:34–43
62. Xiang Y, Li Z, Chen X, Tong A (2008) Highly sensitive and selective optical chemosensor for determination of Cu^{2+} in aqueous solution. Talanta 74:1148–1153
63. Bojinov V, Venkova A, Georgiev N (2009) Synthesis and energy-transfer properties of fluorescence sensing bichromophoric system based on Rhodamine 6G and 1,8-naphthalimide. Sensors Actuators B Chem 143:42–49
64. Lakowicz JR (1991) Topics in fluorescence spectroscopy, Principles, vol 2. Plenum Press, New York
65. Lakowicz JR (1991) Topics in fluorescence spectroscopy, Application, vol 3. Plenum Press, New York
66. Lakowicz JR (1991) Topics in fluorescence spectroscopy, Techniques, vol 4. Plenum Press, New York
67. Irvine DJ, Purbhoo MA, Krogsgaard M, Davis MM (2002) Direct observation of ligand recognition by T cells. Nature 419:845–849
68. Pope AJ, Haupts UM, Moore KJ (1999) Homogeneous fluorescence readouts for miniaturized high-throughput screening: theory and practice. Drug Discov Today 4:350–362
69. Georgiev N, Asiri A, Qusti A, Alamry K, Bojinov V (2014) A pH sensitive and selective ratiometric PAMAM wavelength-shifting bichromophoric system based on PET, FRET and ICT. Dyes Pigments 102:35–45

70. Saleem M, Abdullah R, Ali A, Park B, Choi E, Hong I, Lee K (2014) Synthesis, cytotoxicity and bioimaging of novel Hg^{2+} selective fluorogenic chemosensor. Anal Methods 6:3588–3597
71. Georgiev N, Dimitrova M, Asiri A, Alamry K, Bojinov V (2015) Synthesis, sensor activity and logic behaviour of a novel bichromophoric system based on rhodamine 6G and 1,8-naphthalimide. Dyes Pigments 115:172–180
72. Fabbrizzi L, Licchelli M, Pallavicini P, Perotti A, Taglietti A, Sacchi D (1996) Fluorescent sensors for transition metals based on electron-transfer and energy-transfer mechanisms. Chem Eur J 2: 75–92
73. Dougherty T, Hicks C, Maletta A, Fan J, Rutenberg I, Gafney HD (1998) Excited-state coordination chemistry: a new quenching mechanism. J Am Chem Soc 120:4226–4227
74. Crutchley R, Kress N, Lever ABP (1983) Protonation equilibria in excited-state tris(bipyrazine)ruthenium(II). J Am Chem Soc 105: 1170–1178
75. Giordano PJ, Randolph Bock C, Wrighton MS, Interrante LV, Williams RFX (1977) Excited state proton transfer of a metal complex: determination of the acid dissociation constant for a metal-to-ligand charge transfer state of a ruthenium(II) complex. J Am Chem Soc 99:3187–3189
76. Lei Y, Buranda T, Endicott JF (1990) Photoinduced energy transfer in multinuclear transition-metal complexes. Reversible and irreversible energy flow between charge-transfer and ligand field excited states of cyanide-bridged ruthenium(II)-chromium(III) and ruthenium(II)-rhodium(III) complexes. J Am Chem Soc 112: 8820–8833
77. Said A, Georgiev N, Bojinov V (2019) The simplest molecular chemosensor for detecting pH, Cu^{2+} and S^{2-} in aqueous environment and executing various logic gates. J Photochem Photobiol A Chem 371:395–406
78. Pu F, Ran X, Ren J, Qu X (2016) Artificial tongue based on metal–biomolecule coordination polymer nanoparticles. Chem Commun 52:3410–3413